Landslides (2018) 15:2499–2508
DOI 10.1007/s10346-018-1062-5
Received: 12 May 2018
Accepted: 5 September 2018
Published online: 27 September 2018

Qinwen Tan · Huiming Tang · Lei Fan · Chengren Xiong · Zhiqiang Fan · Meng Zhao · Chun Li · Dingjian Wang · Zongxing Zou

In situ triaxial creep test for investigating deformational properties of gravelly sliding zone soil: example of the Huangtupo 1# landslide, China

Abstract In recent years, numerous landslide catastrophes have occurred, generating considerable financial losses and other tolls. The deformational and mechanical properties of sliding zone soil would be in primary significance to landslide research, as the sliding zone basically controls the initiation and mobility of the landslide. An in situ triaxial test was carried out on a sample from the sliding zone of the Huangtupo 1# landslide, a subdivision of the Huangtupo landslide in the Three Gorges area of China. The test results indicate that (a) the sliding zone exhibits low compressibility due to the high rock content (54.3%) and long-time consolidation by the overlying soil mass; (b) only decaying creep occurs without abrupt failure, and a constitutive equation with both linear and nonlinear viscoplastic terms is deduced to accurately fit the test data; (c) the surface with an orientation of 35° presents anisotropic traits in terms of displacement, possibly due to cracks that formed at similar orientations within the sample cube; and (d) the creep behavior of the landslide may be closely related to the properties of the sliding zone soil. When a similar stress magnitude to that of the in situ stress environment is applied to the sample, the sliding zone soil behavior matches the landslide deformative behavior. The test results indicate that the Huangtupo 1# landslide will continue to creep, as interpreted from the deformation traits and structural properties of the sample. However, unavoidable limitations of the test and extreme external factors, namely unexpected rainfall and water fluctuation, cannot be ignored.

Keywords In situ triaxial creep test · Sliding zone soil · Constitutive law · Anisotropic deformation

Introduction

The sliding zone of a landslide has been recognized as a critical structure that controls the initiation, motion, and even morphology of the landslide. Owning to its significance, studies on the properties of sliding zone soil were common throughout the past few decades, with the intention of gaining a better understand and control of landslides. Traditional testing measures utilized on the sliding zone soil basically consist of shear tests (direct shear and ring shear) and triaxial tests, and most of these tests were conducted by indoor experiments. Indoor experiments have been long recognized due to superiorities such as convenient operation and accurate control, but flaws inevitably exist, mainly due to the following aspects: (a) the samples are structurally disturbed (structural stress lost); (b) the sample constituent is usually changed by screening the sample to achieve a finer mixture; and (c) the size effect that arises due to the apparatus is non-negligible. These flaws have raised the concerns of researchers, who have tested various measures to address them. Chen and Liu (2014) attempted to examine the residual strength of sliding zone soils by in situ direct shear tests; in particular, the apparatus was improved by using a laboratory shear box, and some novel residual shear behaviors were observed. Boldini et al. (2009) conducted large-scale ring shear tests with a DPRI-6 ring shear apparatus developed at the Disaster Prevention Research Institute (DPRI), Kyoto University, to more accurately analyze tsunamigenic landslides. Jiang et al. (2016) emphasized the structure of the sliding zone soil by means of computed tomography (CT) scanning on undisturbed coarse-grained soil and mechanical testing on fine-grained soil. On the other hand, Pirone et al. (2015) and Tang et al. (2014) both intended to reduce experimental errors by combining indoor tests and in situ monitoring to more accurately predict landslides.

Soil deformation develops over time under constant compression and ultimately ceases, depending on the applied stress magnitude, and this process is time consuming. Consolidation theories of the early ages rarely consider the time factor; however, stress and strain always increase with time. Thus, stress-strain equations that do not consider time cannot accurately describe the soil deformation. In this sense, creep test has become increasingly necessary to investigate soil properties, so as to obtain more practical deformational traits and then constitutive laws. Wahls (1962) conducted sets of soil compression tests under diverse loading rates, and the results showed that the primary consolidation was a time-dependent deformation, revealing that creeping also occurred during primary consolidation. Kabbaj et al. (1988) carried out in situ consolidation tests at various low strain rates and a series of indoor tests at normal strain rates, then discovered that the in situ tests exhibited larger deformations than those of the indoor tests. Kabbaj et al. further pointed out that the deformation of a primary consolidation is not immobile, which would be affected by the time duration of the consolidating process. Notably, the above conclusions were drawn only through creep tests that were conducted within a sufficient time duration. Thus, deformation occurs not only during an increase of stress but also during the consolidation and water drainage under constant stress; this trait of the creep test distinguishes creep from normal deformation. These fundamental discoveries have motivated numerous studies on creep tests in recent years, and deeper knowledge of the sliding zone soil properties and deformation has been achieved (Maio et al. 2015; Li et al. 2017).

In recent years, studies on soil deformation traits and stress-strain relationships have become increasingly prevalent (Amiri et al. 2016; Liao et al. 2017), as soil behavior under external forces undoubtedly has a significant impact on engineering practices. However, most stress-strain relationships were determined in laboratories, where in most cases, the soil was disturbed, and the sample was remolded. The internal structure of the sliding zone soil mainly originates from the long-time consolidation that makes the soil matrix dense and cohesive; if the soil is remolded,

loss of internal structure usually leads to a decrease on the strength. This is noteworthy for the sliding zone soil, which is usually buried deep beneath the slope surface, and therefore, the consolidation degree is significant. This question has been discussed by Chen and Liu (2014) who carried out in situ tests and found that the in situ residual strength was less than the peak but greater than the residual strength measured in the laboratory. Similar results were reached by Wen et al. (2016) and Gao et al. (2010), who compared in situ tests with lab tests and reached the same conclusions. Therefore, neglecting the structure destruction would lead to overestimation of the deformation and, as a result, descriptions from the constitutive model may incorporate some errors.

In this paper, the deformation response of sliding zone soil was investigated by means of triaxial testing, where specifically the sample is under the in situ state and remains undisturbed. This is an innovative approach used to learn more about the soil behavior under external force in its natural environment. To implement this testing scheme, a testing tunnel in the Three Gorges area, China, was utilized as the in situ testing site; at this site, the sliding zone of the Huangtupo 1# landslide is exposed.

Background

The Huangtupo landslide

The Huangtupo landslide is located on the south bank of the Yangtze River in the Three Gorges area, and administratively belongs to Badong county, Hubei province, China (see Fig. 1a). The Huangtupo landslide is developed in the strata of the Middle Triassic Badong Formation (T_2b^2 and T_2b^3) and is mainly composed of mudstone, pelitic siltstone, and argillaceous limestone (Tang et al. 2014). The head scarp elevation of the landslide is approximately 600 masl, while the toe varies from 50 to 90 m but is submerged by the Yangtze River. This landslide has a volume of nearly 70 million m^3 and covers an area of 1.35 km^2, making it the largest landslide identified in the Three Gorges area of China.

The landslide was subdivided into four regional landslide areas, namely, the Riverside Slump 1# (Huangtupo 1# landslide), Riverside Slump 2#, Garden Spot Landslide, and Substation Landslide areas, as shown in Fig. 1b. Monitoring data (from GPS and borehole clinometers) indicate that Riverside Slump 1# has deformed the most, meaning that it has the highest risk of failure. A tunnel passing through Riverside Slump 1# was constructed in 2010 (Tang et al. 2014; Hu et al. 2012a, b) to expose the landslide structures, carry out tests, and install monitoring instruments. The tunnel system consists of a main tunnel that stretches approximately 908 m and five branch tunnels (BR-1 to BR-5) stemming from the main tunnel; the tunnel layout is shown in Fig. 1c. The test focused in this paper was carried out at the end of BR-3, where the sliding zone soil was exposed (presented in Fig. 2); other four branch tunnels were not considered for the test mainly due to either not reaching the sliding zone or inconvenient testing environment. A photograph of the test site is shown in Fig. 1c.

Instrument used for in situ triaxial testing

The YXSW-12 instrument was used for the test, which was developed jointly by the Changjiang River Scientific Research Institute (China) and Zhaoyang Experimental Instruments Co., Ltd. (China). The testing system comprises (a) components i.e. a vertical loading unit (jack), horizontal loading unit (hydraulic

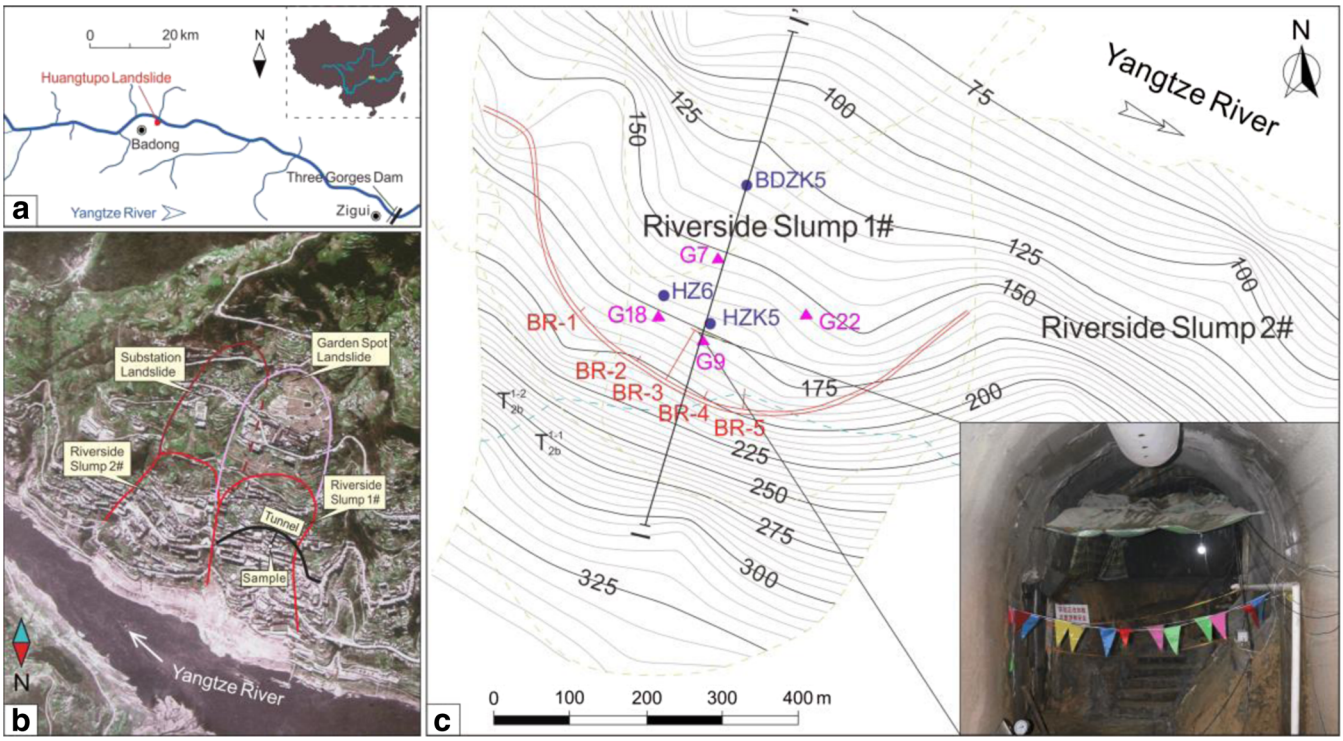

Fig. 1 **a** Location of the study area. **b** Satellite picture showing subdivisions of the Huangtupo landslide. **c** Layout of the testing tunnel in Riverside Slump 1# and picture of the test site (triangles denote GPS points; circles denote boreholes; I-I′ denotes the geological profile)

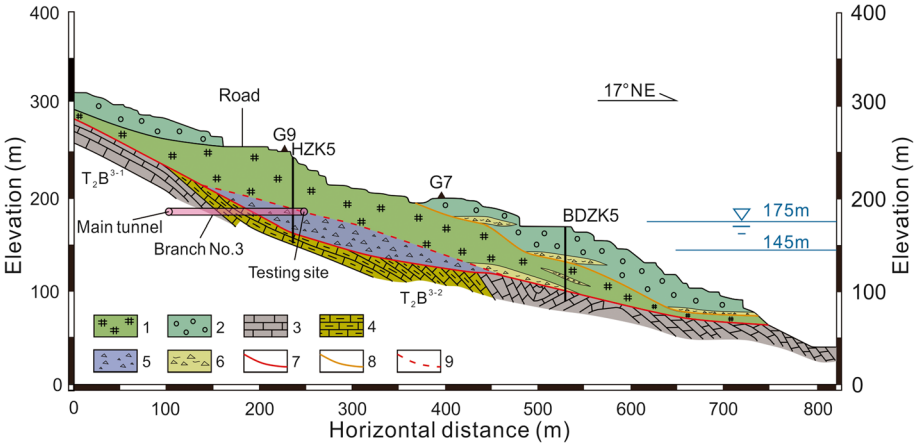

Fig. 2 I-I′ profile of the the Hunagtupo 1# landslide (1-dense soil and rock debris; 2-loose soil and rock debris; 3-limestone; 4-argillaceous limestone; 5-cataclastie; 6-crushed zone; 7-rock-soil interface; 8-local sliding surface; 9-main sliding surface)

pressure pillow), deformation gauge, and counterforce frame, as plotted in Fig. 1 (left), and (b) a power and control unit, composed of a personal computer (PC) that acts as a command center and collects data, an EDC-series servo driver for converting and transmitting the signals, and a servo valve, a booster and an oil source for supercharging the vertical and horizontal loading units. Specifically, the hydraulic pressure pillows expand when charged with oil and exert forces on the soil sample. Horizontal deformation could occur as the pillows would be compressed to deformation under the forces from the creeping soil; during this process, the horizontal pressure would be held constant by the computer-servo system. Specifically, the computer-servo system runs with the connection to the PC, the EDC, the servo valve, and the booster. When the actual stress changes because of external factors, e.g., soil compression and horizontal expansion, the compensation system will automatically detect and then compensate or discharge the pressure by adding or discharging the used oil. The system has also been successfully employed in previous tests by its creation team (Zhang et al. 2011).

The tested cuboid sample had a height of 1000 mm and a cross-sectional area of 500 mm × 500 mm, as presented in Fig. 3. The soil was cut out of the horizontally enveloping soil blocks using a procedure that reduced the disturbance to the soil, and the bottom surface of the cuboid remained connected to the base soil. The four vertical planes of the sample were oriented at 35°, 125°, 215°,

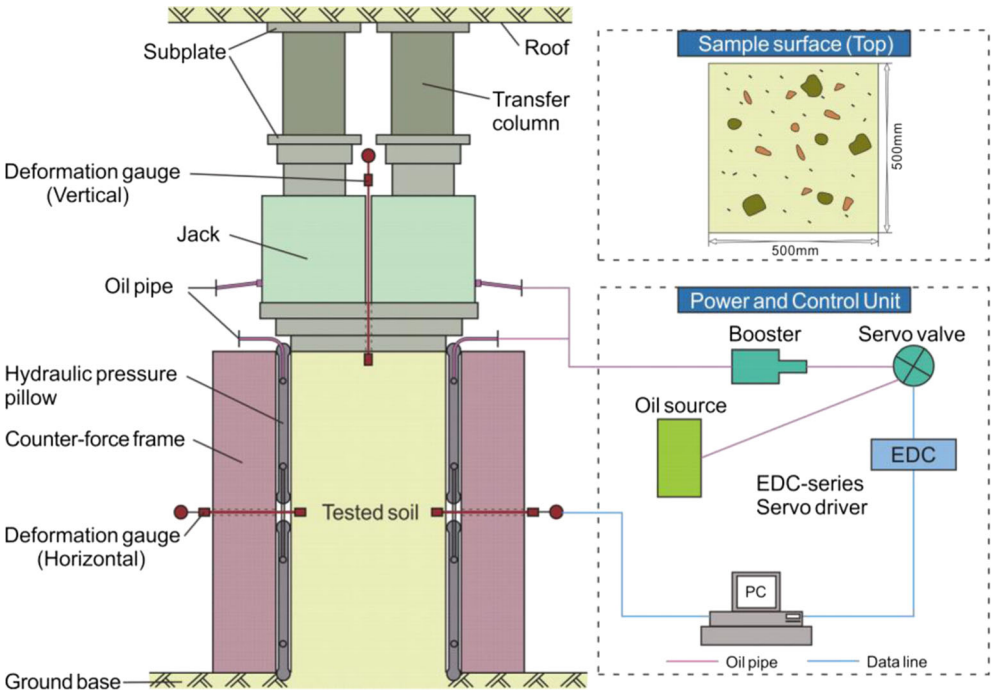

Fig. 3 Structural representation of the YXSW-12 instrument

and 305°, wherein the 35° plane was approximately oriented parallel to the moving direction of the landslide (as plotted in Fig. 4).

Loading scheme and test result

The loading scheme is described using a flow chart, presented in Fig. 5. The confining pressure was kept at 0.5 MPa, which was determined by calculating the initial in situ magnitude based on the horizontal stress coefficient (acquired from previous data); meanwhile, the vertical pressures were increased stepwise from 0.65 MPa (stress level 1) to 0.80 MPa, 0.95 MPa, and 1.10 MPa (stress level 4). The loads, starting with stress level 1, were instantaneously applied on the top surface of the sample, and the subsequent level of stress would be applied when the increase of the displacement approximately ceased.

Deformations of the five sample faces were simultaneously detected by deformation gauges (marked in Fig. 3), and the resultant curves are plotted in Figs. 6, 7, and 8. Figure 6 presents the displacement development curves under stress level 1, in which each face first undergoes an instantaneous elastic deformation and then undergoes an attenuating creep. Specifically, the 35° face quickly deforms by 7 mm in approximately 15 h and then begins an attenuating phase until reaching a steady value at 17.3 mm. The 125°, 215°, and 305° faces deform much like the 35° face, although the magnitudes varies; the total displacements are 1.2 mm, 5.9 mm, and 6.3 mm, respectively. Reasons giving rise to the anisotropic deformation traits of the surfaces would be later discussed in the section "Anisotropic deformation".

The vertical deformation curve from this test also undergoes a linear increase followed by an attenuating creep phase, but the linear phase continues for a much larger time than that of the other faces, nearly 350 h. In total, the vertical displacement during stage 1 (under stress level 1) is 13.6 mm. This phenomenon is unique and can be explained by the following observations. The unsaturated soil undergoes water drainage and volume change under applied forces; therefore, the stress would be transferred to the soil matrix as the water drains out, and the deformation ultimately ceases. This represents a general consolidation process.

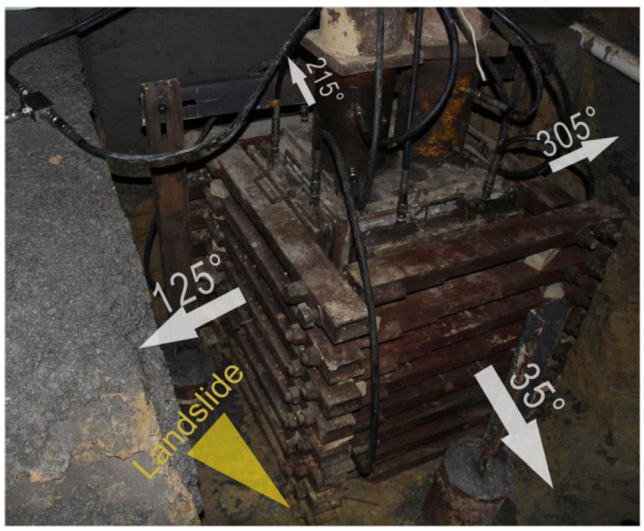

Fig. 4 Orientations of each testing surface and the landslide

In this test, the transient vertical loading on the sample induces a fast pore pressure increase, which concentrates near the loading surface. The pore pressure would thus resist the soil deformation before dissipation is completed. This behavior primarily explains the steady and slow increase in the vertical deformation curve.

As shown in Fig. 5, stress levels 2 and 3 were applied vertically and in succession when the displacement in the former stage had approximately ceased. Figure 7 presents the displacements of all the faces in stage 2 (stress level 2), and Fig. 8 shows the results from stages 3 and 4 (stress levels 3 and 4). These curves are plotted independently for clarity, as the change in displacement during stages 2 to 4 are small; the greatest increases in the deformation curves for stages 2–4 are only approximately 1 mm. Notably, stress levels 3 and 4, respectively, equal and exceed the initial situ stress calculated at the embedment depth of the sliding zone. Therefore, the deformation curves generally exhibit attenuation (Wen and Jiang 2017), indicating that only creep happens, and soil failure will not occur no matter how long creep continues.

Analysis on the low compressibility of the sample

Two factors mainly account for the low compressibility: a high preexisting compression degree of the soil and a high rock content.

High preexisting compression degree

For clay samples, exactly soils for the test, the primary consolidation that normally occurs due to external pressure would stop once the excess pore water pressure has dissipated. However, continuous forces on the soil would ultimately lead to secondary consolidation, enhancing interparticle forces and solidifying some cementing constituents. Clay that undergoes secondary consolidation usually exhibits a higher compression modulus and bears capacity in engineering applications, behaving like "old clay," which refers to clay that formed earlier than the late Pleistocene (Li 2004).

Figure 9 presents two void ratio (e) reduction curves (in blue color) developing with various geological times for the same clay. In Fig. 9, P_o is the applied force for normal consolidation, and e_o is the final void ratio; P_{cq} is a greater stress applied on identical soil, and e_o' equals e_o. The results indicate that compression to T_o under P_o takes 10,000 years; however, under the higher pressure P_{cq}, the time required to reach the same e value (T_{cq}) decreases to less than 0.1 year. Similarly, P_{cq} and P_o curves can serve as a laboratory normally consolidated soil case and a historical consolidation case, respectively. A greater force is needed in the laboratory to reach the density equal to that in historically consolidated soil. We call such historically consolidated soil quasi-over consolidation (QOC) soil, with its quantitative parameter defined as:

$$QOCR = P_o/P_{cq} \tag{1}$$

where QOCR denotes the quasi-over consolidation ratio.

The Huangtupo 1# landslide has a deep-seated sliding zone; consequently, the compressibility of the sliding zone soil tends to be smaller than that of a normally consolidated soil from a laboratory experiment, as QOC can create a denser soil structure.

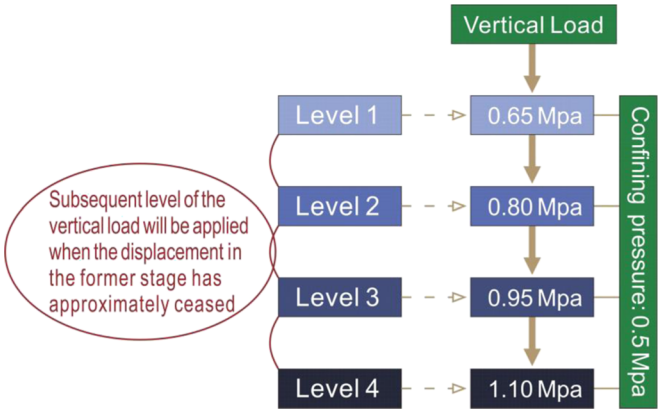

Fig. 5 Flow chart of the loading scheme

High rock content

Rock content considerably affects soil compressibility. Xu et al. (2009) discovered, after testing samples with rock contents of 30%, 40%, 50%, and 60%, that the uniaxial compressive strength (UCS) of soil samples monotonically increases with the rock content. Tests by Li and Wang (2004) showed that gravelly soil with low rock contents (< 30%) behaved like a pure soil; conversely, gravelly soil with high rock contents (> 60%) behaved like a rock mass.

In this test, the rock blocks generally have a sparse to dense distribution from the sample top to the bottom, and the total rock content (particle diameter > 5 mm) reaches 54.3% in the sample cube. Therefore, the cube is characterized as gravelly soil with inhomogeneously embedded rock blocks. As demonstrated by previous studies, the compressibility of soils decreases with the increase in rock content in the soil mass, due to the following reasons: (a) when neighboring rocks obstruct each other during shearing, the soil movement is locked. (b) Peculiarly located rocks have the potential to block the development of shear zones and cracks. Some test results suggest that once the rock content exceeds 50%, the largest rocks in the soil generally determine the shear zone shape and location and mechanical properties (Xu et al. 2009).

Constitutive law

The preceding constitutive laws for soil samples involve two limitations: (a) a time term is rarely addressed in the equation and (b) the samples are generally tested in laboratories, where they contain finer grains and are characterized at small scales. In this paper, a time term is incorporated into the constitutive equation to establish a stress-strain-time relation for a sample under compression.

Elements for the constitutive equation

The constitutive equation that includes a linear viscoplastic element and nonlinear viscoplastic element is considered for the sample. Specifically, the linear viscoplastic element is reflected by the assembly of rheology bodies frequently used for studying soil behavior; empirical equations will be introduced to describe the nonlinear viscoplasticity, which cannot be described by the rheology bodies. In general, rheology bodies can be categorized as follows:

a. Hooke's body (abbreviated as H), depicted as a mechanical spring, introduces linear relations between stress and strain, irrespective of time.

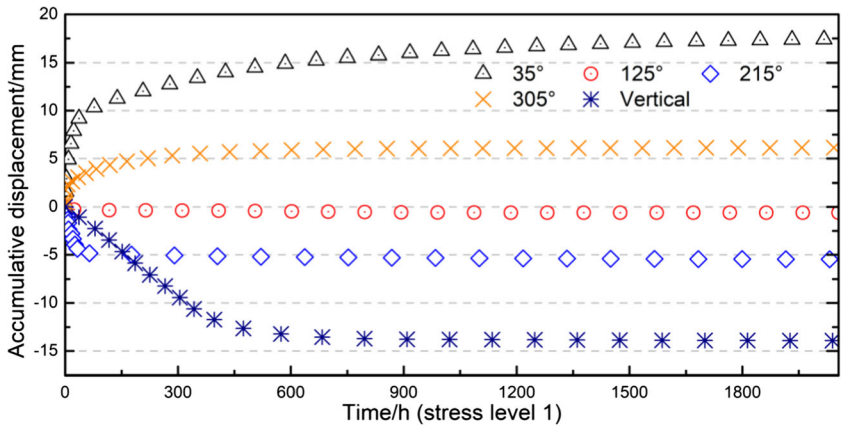

Fig. 6 Displacement-time curves of the 5 surfaces under stress level 1. Negative values indicate shrinking deformation, which is discussed in the section "Anisotropic deformation"

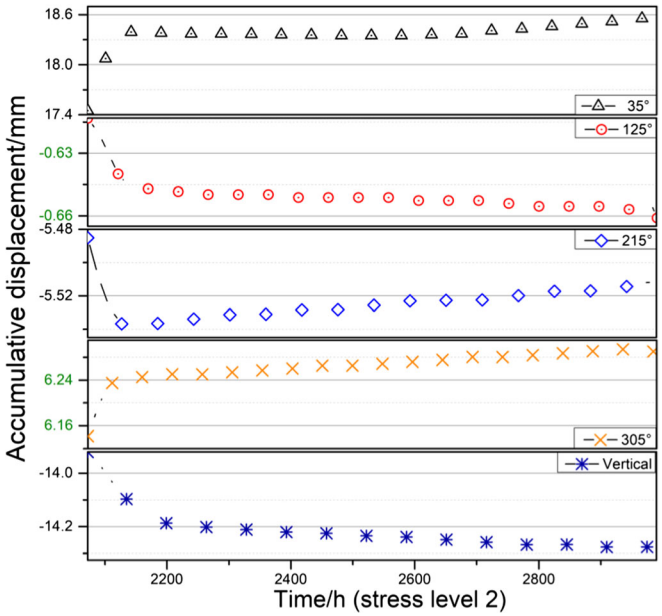

Fig. 7 Displacement-time curves of the 5 surfaces under stress level 2

b. Newton's body (N), depicted as a piston with an annular tube that holds viscoplastic liquid, describes viscoplastic deformations by incorporating a time factor.
c. Saint Venant's body (ST.V), depicted as two blocks that are in contact and have rough surfaces, reflects the plasticity during deformation.>

Viscoelastic deformation is not incorporated in the constitutive equation as an independent term because it is not clearly displayed in the deformation data, and also usually exhibits apparent linearity. Reasons of lacking the viscoelastic deformation may well be due to the pre-existing vertical pressure on the sample from the overlying soil, which had lasted long during the historical period. Elastic deformation already occurred much in the historical period, but no obvious rebound took place owning to the creep generated by the long-time vertical load acting on the soil. Thus, the long-time and high-intensity compression on the soil caused irreversible creep that may account for a considerable proportion of the deformation. Consequently, the configuration

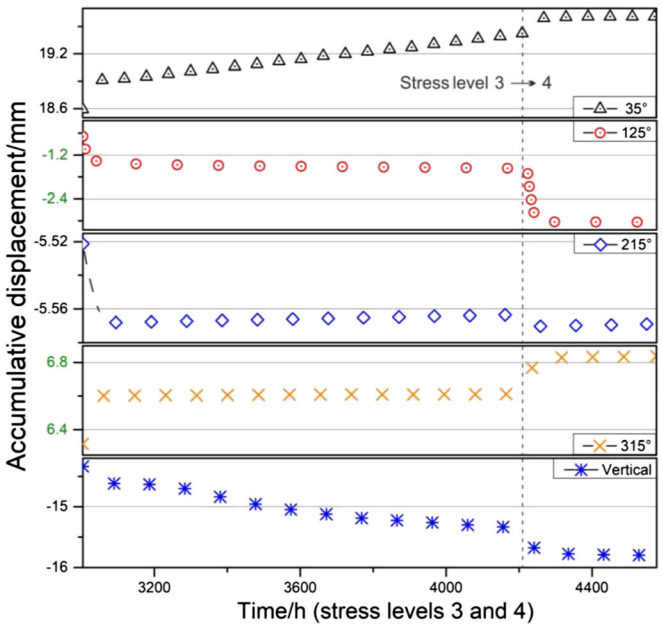

Fig. 8 Displacement-time curves of the 5 surfaces under stress levels 3 and 4. An abrupt change can be observed in each curve at the start of stage 4

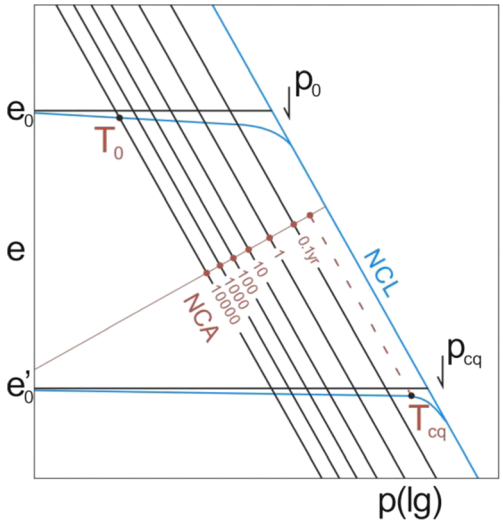

Fig. 9 Void ratio (e) reduction curves developing with various geological times, where NCL denotes the natural consolidation line and NCA denotes the natural consolidation age (Li 2004)

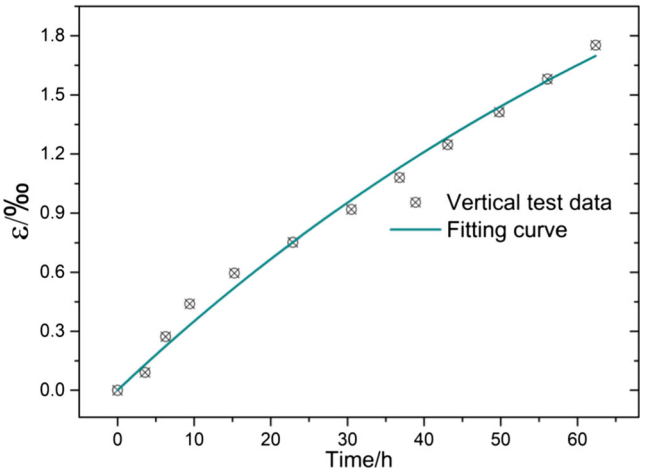

Fig. 11 Fitting result for linear viscoplastic segment

is shown in Fig. 10, where a term of linear viscoplasticity and a term of nonlinear viscoplasticity are connected in series (Wang 2007; Zheng 2016); notably, the linear viscoelasticity term (dashed) is excluded from the constitutive equation.

Linear viscoplasticity term

Based on previous studies, the linear viscoplasticity term can be written as:

$$\varepsilon_l = \frac{\sigma - \sigma_s}{E_l}\left(1 - \exp\left(-\frac{E_l}{\eta_l}t\right)\right) \tag{2}$$

where E_l and η_l denote the elasticity modulus and viscosity coefficient of the rheology bodies, respectively. σ_s denotes the yield stress of the soil.

Eq. (2) can be transformed as:

$$y = a_1(1 - \exp(-b_1 x)) \tag{3}$$

where $a_1 = (\sigma - \sigma_s)/E_l$, $b_1 = E_l/\eta_l$.

Thus, we use a_1 and b_1 to create a more concise equation for the linear viscoplasticity term, as given by Eq. (3). Notably, a_1, which can be defined by σ, σ_s, and E_l, can be treated as an integrated coefficient; if σ is known and σ_s is fixed, then E_l is the only unknown variable. Furthermore, the linear-nonlinear boundary of each displacement-time curve is ascertained based on the shape of the curve that is created by the critical points of the linear-nonlinear boundary. Therefore, Eq. (3) is tested to match the linear viscoplasticity data using the fitting function of *Origin* developed by *OriginLab* of the US. The data employed here are from the first stage (stress level 1).

Figure 11 plots the fitting results, where the correlation coefficient of determination (r^2) is 0.9910, signifying a high correlation. In this sense, the term consisting of paralleled H, N, and ST.V bodies is proven to be effective in reflecting the linear viscoplasticity of the soil.

Nonlinear viscoplasticity term

The nonlinear viscoplasticity term can be expressed by an empirical model that reflects such deformation traits. Empirical models frequently adopted for describing the rheological behavior generally include the power function, exponential function, and logarithmic function. Specifically, the power function is usually used for reflecting the decaying creep; the exponential function, for steady creep; and the logarithmic function, for accelerating creep. In this sense, the power function is selected to describe the decaying creep in this test, expressed as:

$$\varepsilon_n = \left(\frac{\sigma - \sigma_s}{A}\right)^m \tag{4}$$

where $m = 1/m'$ and $m > 1$.

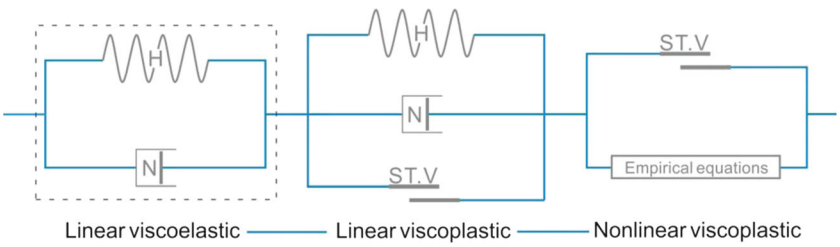

Fig. 10 Configuration of the constitutive equation. The term inside the dashed rectangle is eliminated

Nonlinear viscoplastic creep relaxes with time; thus, A and m in Eq. (4) should be time-related parameters, which can be written as:

$$A = A(t), m = m(t) \tag{5}$$

$A(t)$ can also be represented by a power function (Sun 1999), which can be expressed as:

$$A(t) = A_0 t^{-\alpha} \tag{6}$$

Then, Eqs. (4) and (6) are combined so that the nonlinear viscoplasticity term can be finally obtained:

$$\varepsilon_n = \left(\frac{\sigma-\sigma_s}{A_0 t^{-\alpha}}\right)^m = \left(\frac{\sigma-\sigma_s}{A_0}\right)^m t^{\beta} \tag{7}$$

where β is the creep index, $\beta = m\alpha$, and A_0 is the nonlinear coefficient of the deformation.

Expression of the constitutive model

The final expression of constitutive law can be obtained through series connection of two terms (Wang 2007; Zheng 2016), respectively, of linear viscoplasticity and nonlinear viscoplasticity, and the equation is written as:

$$\varepsilon = \frac{\sigma-\sigma_s}{E_l}\left(1-\exp\left(-\frac{E_l}{\eta_l}t\right)\right) + \left(\frac{\sigma-\sigma_s}{A_0}\right)^m t^{\beta} \tag{8}$$

Likewise, fitting is conducted employing the *Origin* and the result is shown in Fig. 12. The coefficient of determination (r^2) turns out 0.9768, indicating that the created model is convictive to match the test data. Therefore, Eq. (8) is ultimately determined to interpret the constitutive law of the tested sample.

It is noteworthy that Fig. 12 displays only the fitted data of the first stage (stress level 1), mainly because those data possess manifest linear and nonlinear courses of deformation, and thus, the random errors can be shrunk to the minimum. Further, Eq. (8) is utilized to fit the data, respectively, of stages 2, 3, and 4, and the data prove to be well fitted as well (not displayed in the text).

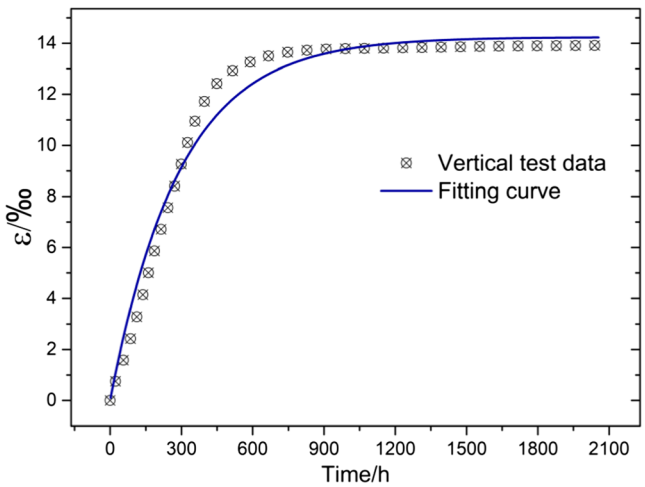

Fig. 12 Fitting result for the intact data during stress level 1

Anisotropic deformation and landslide movement

Anisotropic deformation

The displacement-time curves presented in Figs. 6, 7, and 8 indicate that strain is directionally favoring the 35°, 215°, 305° and vertical surfaces, respectively. Specifically, the 35° surface expands the most among the horizontally oriented surfaces, reaching approximately 3 times the amount of displacement at the 215° and 305° surfaces.

When compressed by vertical stress, the high rock content in the soil would enable the sample to behave like a rock mass. That is, cracks may emerge at locations of concentrated stress and at the soil-rock interfaces, where the cementation is weakest. For the tested sample, the areas of concentrated stress are generally oriented along the $45^\circ + \phi/2$ direction (marked in Fig. 13), along which the generated shear strength is generally the greatest for a compressed cube. Additionally, as the rock content (particle diameter > 5 mm) reaches 54.3% of the soil-rock mixture, the numerous soil-rock interfaces in the sample induce cracks widely distributed throughout the sample.

The 35° surface is similar to the landslide orientation (see Fig. 4). As has been previously discussed, particles within the sliding zone would gradually align with the sliding direction after long-time creep and movement of the soils and rocks. Therefore, cracks that form at the soil-rock interfaces would also be oriented at 35°, and ultimately, a weakness develops along this orientation, explaining why the 35° surface deforms much more intensely than the other surfaces.

The 215° surface, however, presents a shrinkage trait (negative displacement in Figs. 6, 7, and 8) under the joint action of a vertical load and constant confining pressure of 0.5 MPa. With respect to the cracks mentioned above, because the soils and rocks generally move towards the orientation of 35°, a shrinkage in that orientation is expected. The 125° and 305° surfaces are also expected to be characterized with a distribution of cracks, which would result in an inhomogeneous shear strength under compression; specifically, orientations of the main cracks (35°) may have components to the orientation of 125°, which is estimated from the intersection angle between the sliding direction and the 35° orientation (plotted in Fig. 4). Therefore, the deformations of these surfaces would be very different.

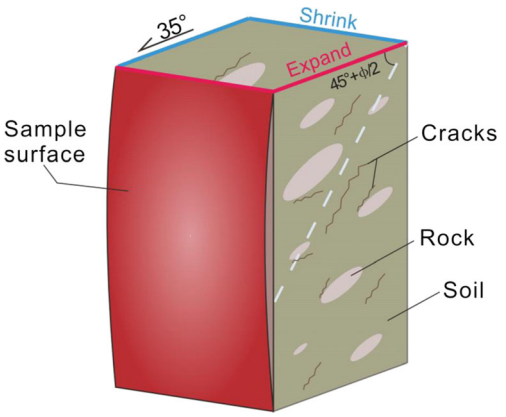

Fig. 13 Schematic diagram showing the deformed 35°-oriented surface of the cube and structures within the cube after testing

Landslide movement related to the sample

The Huangtupo 1# landslide has been monitored since 2003; various measures including the use of GPS, borehole drilling, and time-domain reflectometry (TDR) have been employed for monitoring efforts. Some monitoring sites on the Huangtupo1# landslide are presented in Figs. 1 and 2; these sites are distributed not far from tested sample. The monitoring measures shown in Fig. 1 consist of GPS sites and boreholes; specifically, the GPS sites are responsible for detecting deformation of the slope surface, and boreholes were drilled into the sliding zone and instrumented to detect the deformation of the sliding zone. Monitoring data are presented in Fig. 14.

G9 is located above the sample, and the average deformation velocity at this location is 22.97 mm/year, while the average deformation velocities for the data curves in Fig. 14 range from 13.71 mm to 26.78 mm/year. HZK5 extends to the sliding zone soil positioned very close to the tested sample, as clearly marked in Fig. 14 with a dotted line. The calculated deformation velocity at HZK5 is 10.65 mm/year.

The displacement developed under stress level 3 (see Fig. 8) is selected to represent the deformation velocity of the soil cube because the stress applied in the third stage (0.95 MPa) equals the in situ overlying load, which can be estimated from the burial depth of the sample and the soil gravity of the sliding mass. At this time, the sample enters into a sustained nonlinear viscoplastic phase, consistent with the ordinary state for soil creeping. The calculated velocity is 5.84 mm/year for the 35°-oriented surface, whose normal direction is basically parallel to the landslide direction, as explained in the previous section.

The deformation laws of the soil cube and the sliding zone are compared, as a similar stress environment was considered for both the confining pressures and the vertical loads. Nonetheless, a distinction of approximately 5 mm appears between the detected velocity from HZK5 and the calculated velocity for the sample, even though they are located very close to one another. This phenomenon may be due to external factors, namely, rainfall and water level fluctuations. The impacts of these factors have been demonstrated to be significant for the Huangtupo 1# landslide. Wang et al. (2016) investigated the roles on the deformation of the Huangtupo 1# landslide played by rainfall and water level fluctuation, with the results indicating that approximately half of the total deformation was attributed to rainfall and water level decrease. Therefore, the final velocity to be evaluated must take rainfall and water fluctuation (presented in Fig. 14) into account.

The data indicates, to some extent, that deformation decreases from the landslide surface to the sliding zone. In addition, the landslide undergoes creeping without a high risk of abrupt failure, as determined by the attributes of the sliding zone soil. As previously analyzed, the sliding zone possesses very low compressibility due to its high rock content and high degree of historical consolidation. The applied vertical force, which is even higher than the original stress induced by the overlying soil, cannot cause the abrupt failure of the sliding zone soil. That is, the Huangtupo 1# landslide has been creeping for years, and this will not change under normal circumstances. Nonetheless, extreme conditions for rainfall and water fluctuation in the Three Gorges Reservoir area must be considered, as they may generate problems such as a considerable increase in the hydrodynamic pressure and water content, possibly leading to failure.

However, further discussion is still requested on the topic. As the sample tested is merely situated near the mid location of the sliding surface, the possibility of reflecting the intact sliding zone should be further addressed. On this issue, some discussions would be given in the following:

a. The intact sliding zone is embedded beneath the homogeneous material of the landslide mass, which can be clearly seen from Fig. 2. In this sense, it is reasonable to consider that the whole sliding zone soil has no much difference in terms of the deforming traits and mechanism compared with the tested sample.
b. The landslide has been creeping for years according to data from the monitoring sites, which are installed widely on the landslide surface (Wang et al. 2016). Therefore, creeping keeps occurring within the whole landslide. In this sense, behavior of other locations can be positively analyzed based on the test in this paper.>

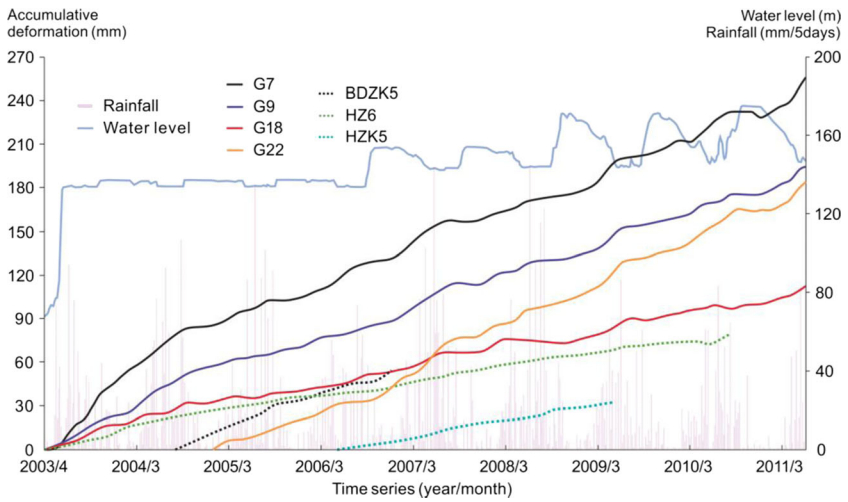

Fig. 14 Time series monitoring data from 2003 to 2011

Conclusions

An in situ triaxial creep test was carried out for investigating the properties of the sliding zone soil, which is characterized by a high rock content and high degree of compression. The tested sample was situated in the tunnel that passes through Riverside Slump 1#, a subdivision of the Huangtupo landslide. The test was completed over 191 days, and the results were then analyzed. The conclusions are as follows:

a. The tested sample exhibits very low compressibility due to the high rock content (54.3%) and long-time compression exerted from the overlying soil. The dense structure leads to a high strength and stability, such that the creep test results in only decaying creep.
b. The constitutive model of the vertical stress-strain-time relationship is discussed and deduced. Linear viscoplasticity and nonlinear viscoplasticity terms are used in series to establish the equation, where an empirical model (power function) is combined to more accurately describe the nonlinear viscoplasticity. The results show a strong fitting relation between the testing data and the constitutive model.
c. The anisotropic traits of the horizontal deformation of the sample are discussed. The surface at an orientation of 35° generates much larger displacement than those at the other surfaces, possibly attributable to the alignment of cracks within the sample cube.
d. The monitored data from HZK5 behave similarly to the measured data from the 35° surface in terms of the velocity of displacement. The data from the GPS sites and boreholes indicate that the Huangtupo 1# landslide has been creeping over the past years. This creep may be controlled by the properties of the sliding zone: decaying creep occurs and no abrupt failure occurs in the tested sample when stress magnitudes similar to those of the in situ stress environment are applied. However, unavoidable limitations of the test and extreme external factors, such as unexpected rainfall and water fluctuation in the Three Gorges area, cannot be neglected when evaluating the long-time stability of the Huangtupo 1# landslide.>

Acknowledgements

The authors would like to appreciate Prof. Koyji Sassa, secretary general of the International Consortium on Landslides (ICL), for his helpful suggestions.

Funding information

This study was financially supported by the National Key R&D Program of China (grant number 2017YFC1501305), Key National Natural Science Foundation of China (grant number 41230637), and National Natural Science Foundation of China (grant number 41502290 and 41702319).

References

Amiri SAG, Grimstad G, Kadivar M, Nodar S (2016) Constitutive model for rate-independent behavior of saturated frozen soils. Can Geotech J 53(10):1646–1657

Chen XP, Liu D (2014) Residual strength of slip zone soils. Landslides 11(2):305–314

Boldini D, Wang FW, Sassa K, Tommasi P (2009) Application of large-scale ring shear tests to the analysis of tsunamigenic landslides at the Stromboli volcano, Italy. Landslides 6(3):231–240

Gao ZB, Gao YF, Tan HM (2010) Lab and in-situ tests on maximum dynamic shear modulus of saturated clay soils. Chin J Geotech Eng 32(5):731–735 (in Chinese with English abstract)

Hu XL, Tang HM, Li CD, Sun RX (2012a) Stability of Huangtupo I# Landslide under Three Gorges Reservoir Operation. Appl Mech Mater 170-173:1116–1123

Hu XL, Tang HM, Li CD, Sun RX (2012b) Stability of Huangtupo Riverside Slumping mass II# under water level fluctuation of Three Gorges Reservoir. J Earth Sci China 23(3):326–334

Jiang JW, Xiang W, Rohn J, Schleier M, Pan JJ, Zhang W (2016) Research on mechanical parameters of coarse-grained sliding soil based on CT scanning and numerical tests. Landslides 13(5):1216–1272

Kabbaj M, Tavenas F, Leroueil S (1988) In situ and laboratory stress–strain relationships. Géotechnique 38(1):83–100

Li C, Tang HM, Han DW, Zou ZX (2017) Exploration of the creep properties of undisturbed shear zone soil of the Huangtupo landslide. Bull Eng Geol Environ:1–12

Li GX (2004) Advanced soil mechanics. Tsinghua Press, Beijing (in Chinese)

Liao MK, Lai YM, Liu EL, Wan XS (2017) A fractional order creep constitutive model of warm frozen silt. Acta Geotech 12(2):377–389

Li SH, Wang YN (2004) Stochastic model and numerical simulation of uniaxial loading test for rock and soil blending by 3D - DEM. Chin J Geotech Eng 26(2):172–177 (in Chinese with English abstract)

Maio CD, Scaringi G, Vassallo R (2015) Residual strength and creep behaviour on the slip surface of specimens of a landslide in marine origin clay shales: influence of pore fluid composition. Landslides 12(4):657–667

Pirone M, Papa R, Nicotera MV, Urciuoli G (2015) In situ monitoring of the groundwater field in an unsaturated pyroclastic slope for slope stability evaluation. Landslides 12(2):259–276

Sun J (1999) Rheology of rock and soil materials and its engineering application. China Architecture and Building Press, Beijing (in Chinese)

Tang HM, Li CD, Hu XL, Su AJ, Wang LQ, Wu YP, Criss R, Xiong CR, Li YA (2014) Evolution characteristics of the Huangtupo landslide based on in situ tunneling and monitoring. Landslides 12(3):511–521

Wahls HE (1962) Analysis of primary and secondary consolidation. ASCE 88(6):207–234

Wang B (2007) Research on the interaction of coupling seepage and stress and deformation of landslide the condition of water level fluctuation. Dissertation, China University of Geosciences, Wuhan, China

Wang JE, Su AJ, Xiang W, Yeh HF, Xiong CR, Zou ZX, Zhong C, Liu QB (2016) New data and interpretations of the shallow and deep deformation of huangtupo no. 1 riverside sliding mass during seasonal rainfall and water level fluctuation. Landslides 13(4):795–804

Wen BP, Jiang XZ (2017) Effect of gravel content on creep behavior of clayey soil at residual state: implication for its role in slow-moving landslides. Landslides 14:559–576

Wen Y, Yang GH, Tang LS, Xu CB, Huang ZX, Huang ZM, Zhang YC (2016) Tests and parameters study of mechanical properties of granite residual soil in Guangzhou area. Rock and Soil Mechanics 37(Supp 2):209–215 in Chinese with English abstract

Xu WJ, Hu RL, Yue ZQ (2009) Development of random mesostructure generating system of soil-rock mixture and study of its mesostructural mechanics based on numerical test. Chin J Rock Mechan Eng 28(8):1652–1665

Zhang YH, Zhou HM, Zhong ZW, Xiong SH, Hao QZ (2011) In situ rock masses triaxial test system YXSW–12 and its application. Chin J Rock Mech Eng 30(11):2312–2320 (in Chinese with English abstract)

Zheng J (2016) Research on the consolidation properties of saturated remolded clay considering the timeliness. Dissertation, Chang'an University, Xi'an, China

Q. Tan · H. Tang (✉) · Z. Fan · M. Zhao · C. Li · D. Wang
Faculty of Engineering,
China University of Geosciences,
Wuhan, 430074, Hubei, China
Email: tanghm@cug.edu.cn

H. Tang · C. Xiong · Z. Zou
Three Gorges Research Center for Geo-hazards of Ministry of Education,
China University of Geosciences,
Wuhan, 430074, Hubei, China

L. Fan
Key Laboratory of Geotechnical Mechanics and Engineering of the Ministry of Water Resources, Yangtze River Scientific Research Institute,
Wuhan, 430019, Hubei, China